J. Fluid Mech. (1989), *vol.* 209, *pp.* 639–660
Printed in Great Britain

Growth and translation of a liquid–vapour compound drop in a second liquid. Part 2. Heat transfer

By S. T. VUONG AND S. S. SADHAL
Department of Mechanical Engineering, University of Southern California, Los Angeles, CA 90089-1453, USA

(Received 21 March 1989)

The present work is a comprehensive theoretical study of the heat transfer associated with a 3-singlet compound drop that is growing because of change of phase. The geometry is the same as in Part 1, i.e. a vapour bubble partially surrounded by its own liquid in another immiscible liquid. The attempt here is to gain fundamental understanding of the transport processes that take place in connection with direct-contact heat exchange. The fluid dynamics associated with its growth and translation is treated in Part 1. Here, that flow field solution is used to obtain the temperature field and hence the evaporation rate. The energy equation for the system consisting of a single compound drop is solved numerically by finite-difference methods. The results give the complete time history of evaporation of the drop. In addition, useful quantities such as the Nusselt number are given and compared with existing experimental data. Most of the results have good agreement with experimental data.

1. Introduction

In Part 1 (Vuong & Sadhal 1989), we studied the basic fluid dynamics associated with a 3-singlet compound drop with growth and translation. As mentioned there, these types of compound drops arise in the area of direct-contact heat exchange and the 3-singlet (3-S) configuration corresponds to the situation in which the dispersed phase consists of a vapour bubble partially surrounded by its own liquid. In the present paper we utilize the flow field results to solve the heat transfer problem for an evaporating compound drop. The analysis in this paper specifically deals with the 3-S configuration.

Before considering direct-contact heat exchange, we briefly describe the bubble nucleation mechanism. The evaporation of a drop, or bubble nucleation in a drop, is classified into two categories: homogeneous nucleation and heterogeneous nucleation. Homogeneous nucleation generally takes place when the liquid is purified to remove all contaminants and degassed to eliminate all microscopic gas pockets that may exist in the liquid. When the liquid is in a homogeneous phase, the vapour will not appear at the equilibrium temperature corresponding to the ambient pressure but will be superheated. In order for the vapour phase to exist, sufficient energy is needed to create the liquid–vapour interface. This requires the liquid to be superheated to a certain degree. A homogeneous liquid at one atmosphere can be heated up to 90% of its critical temperature without any nucleation taking place. The temperature at which nucleation begins is called the limit of superheat, which is important to know when defining safety guidelines to reduce hazards in industry since homogeneously nucleated liquids boil with violent explosions.

Heterogeneous nucleation is a nucleation process in which the liquid medium contains vapour or entrapped gas that exist with impurities such as dust particles. These vapour or gas pockets, even though their size may be microscopic, are generally larger than the critical size for nucleation to take place. Therefore, if the liquid is slightly superheated, it will evaporate into the gas or vapour pockets completely so that the system can stay at a minimum chemical potential. To calculate the required amount of superheat, one can use the Clausius–Clapeyron equation combined with the pressure–radius relation:

$$T_{\mathrm{L}} - T_{\mathrm{sat}} = \frac{T_{\mathrm{sat}}}{\rho_{\mathrm{v}} h_{\mathrm{fg}}} \frac{2\sigma}{R}, \tag{1}$$

where $2\sigma/R$ represents the pressure difference between the liquid and the vapour bubble. We can see that the heterogeneous nucleation requires a negligibly small amount of superheat. In direct-contact heat exchange or any practical engineering applications, the fluids used always contain a certain degree of impurity and therefore the heterogeneous nucleation process prevails and is the subject of the present study. It is also understood that in practical situations a high degree of superheat is likely to be present. The validity of the analysis here is restricted to low superheat owing to the limitation of Stokes flow. The situation being investigated is, nevertheless, physically realizable.

Direct-contact heat exchange occurs when immiscible fluids are brought into contact, resulting in the evaporation of the fluid that has a lower boiling point. Direct-contact heat exchange has been studied by many researchers because it has many advantages over conventional heat exchangers, such as the elimination of the solid wall between fluids resulting in saving of material cost, higher rate of heat transfer because of larger contact area between the fluids, the ability to operate at small temperature difference, and the elimination of corrosion and scaling problems associated with the heat transfer surfaces. Applications of direct-contact heat exchange includes power generation, ocean water desalination, geothermal heat recovery and thermal energy storage systems. A general method used in direct-contact heat exchange consists of injecting drops of a volatile liquid (dispersed phase) into a column of an immiscible liquid (continuous phase) whose temperature is above the boiling point of the drops. The drops will travel up the column, evaporate and change shape simultaneously. In order to obtain an optimal design, a good understanding of fluid mechanics and heat transfer to such drops is necessary for sizing direct contact boilers and condenser.

The motion of a vapour bubble, partially engulfed by its own liquid in an immiscible liquid (i.e. 3-S configuration) has been studied experimentally and theoretically by Hayakawa & Shigeta (1974) and also by Tochitani, Mori & Komotori (1977*a*) and Tochitani *et al.* (1977*b*). They assumed the drop to be of spherical shape in their theoretical analysis and applied Stokes drag to obtain the terminal velocity. Selecki & Gradon (1976) and Gradon & Selecki (1977) integrated the one-dimensional momentum equation to obtain the travel distance of the drop as a function of time. A similar solution was also obtained by Mokhtarzadeh & El-Shirbini (1979), and by Battya, Raghavan & Seetharamu (1984).

The heat transfer characteristics of a partially engulfed gas–liquid compound drop translating in a different immiscible fluid appear to have been first studied by Klipstein (1963) who obtained experimentally the heat transfer coefficients with an evaporating drop of ethyl chloride in a glycerine–water and aerosol–water solution. Prakash & Pinder (1967*a*, *b*) used a cine-photographic technique to study the

evaporation of single drop of furan, cyclopentane and isopentane rising in water. Later, Adams & Pinder (1972) obtained the average heat transfer coefficients for the evaporation of drops of isopentane and cyclopentane in different glycerine–water solutions.

Among the earlier pioneering studies, Sideman & Taitel (1964) used pentane and butane drops as the dispersed phase evaporating in continuous phase of distilled and sea water. They also developed an analytical expression for the Nusselt number by solving a steady-state energy equation assuming potential flow for the continuous phase, but ignored the heat transfer and fluid flow for the dispersed phase. They assumed the drop to be of spherical shape, which is an approximation and applicable only to a limited type of fluid system. Because of these simplifying assumptions, their prediction matched the experimental data only at the final stage when the drop has almost evaporated. The liquid portion of the drop is small and thin so that their assumption is valid in this region. At the early stage when the drop consists mostly of liquid, Sideman & Taitel's (1964) model overpredicted the heat transfer rate because of the neglected thermal resistance of the drop and the associated transient effect. Experimental studies on a butane drop rising in brine were carried out by Simpson, Beggs & Nazir (1974). In addition to evaporation, they observed an oscillation of the drop causing the liquid butane to slosh from side to side, forming a thin film of liquid butane over the top of the inside bubble surface. The oscillation of the rising bubble is probably caused by the periodic vortex shedding of the wake due to higher Reynolds number, resulting in change of shape of the drop from spherical through ellipsoidal to a cap-shaped bubble. In order to avoid the zigzag trajectory that a rising drop has to undergo in low- and moderate-viscosity fluids, Tochitani *et al.* (1977*a*, *b*) used a highly viscous fluid as continuous phase. By using glycerol as the continuous phase, they were able to maintain the pentane drop close to a spherical shape and the drop rose in a rectilinear manner from the initial to the final states. They handled the theoretical aspects of the problem by using a method and assumptions similar to the ones used by Sideman & Taitel (1964) except that the fluid flow field was replaced by the Stokes solution for a sphere. For the heat transfer part, Tochitani *et al.* (1977*a*, *b*) also assumed a quasi-steady state by neglecting the transient term in the energy equation, which was not a good approximation since the Péclet number associated with this term is large (of the order of 100). Their model predicted a total heat transfer rate in a fashion which is very similar to that of Sideman & Taitel's (1964) model. More recent studies include Raina & Grover (1982, 1985), Raina, Wanchoo & Grover (1984) and Raina & Wanchoo (1986). Their models are also similar in many respects to the models by Sideman & Taitel (1964) and Tochitani *et al.* (1977*a*, *b*) with modification to the boundary conditions. Tadrist *et al.* (1987) studied the vaporization of a single drop and applied it to multidroplet systems. The evaporative cooling of liquid drops has been studied by Mori *et al.* (1981). They formed compound drops by coating the liquid drops to be cooled with a volatile liquid and applied evaporative cooling in the atmosphere.

In connection with direct-contact condensation of vapour bubbles, Jacobs & Major (1982) studied the collapse of compound drops. They took into consideration the heat and mass transfer in the gas phase and demonstrated the importance of non-condensibles when these are present. Later, Lerner & Letan (1985) examined the condensation problem when there is a thin condensate film. Oğuz & Sadhal (1987) investigated both condensation and evaporation of a 2-singlet compound drop in considerable detail. A lot of effort has also been put into understanding the problems associated with direct-contact condensation on liquid drops in a gaseous continuous

phase. Specifically, Chung & Ayyaswamy (1981) and Chung, Ayyaswamy & Sadhal (1984*a*, *b*) have studied the laminar condensation on a slowly translating water drop in a steam–air mixture. Subsequent developments in a higher-Reynolds-number regime were carried out by Sundararajana & Ayyaswamy (1984).

While significant progress has been made with previous models, there has been a lack of rigorous analysis, presumably due to the complicated fluid dynamics. This difficulty has been overcome in Part 1, at least in the creeping-flow regime. The purpose of the present work is to carry out a comprehensive study of the heat transfer of a compound gas–liquid drop using the flow field developed in Part 1. Here we numerically solve the energy equation including the conduction, the convection and the transient terms for both the continuous and dispersed phases. The results of the analysis are compared with existing experimental data obtained by Tochitani *et al.* (1977*a*, *b*) using pentane as the dispersed phase and glycerol as the continuous phase. In the following sections, we shall give a detailed description of the problem and state the governing equations, followed by the analysis, and finally, results and discussion.

2. Statement of problem

We are considering here the situation in which a liquid drop is injected into another hotter immiscible liquid with a higher boiling point. There is sufficient superheat to allow heterogeneous nucleation of the liquid drop. The vapour then grows, and at the same time the compound drop thus formed (see figure 1) translates owing to buoyancy. Since the change of phase takes place slowly, the thermodynamic equilibrium approximation can be made at the liquid–vapour interface. This assumption requires the liquid–vapour interface and the vapour phase to be at the equilibrium temperature corresponding to the hydrostatic pressure. As a result, the vapour is effectively decoupled from the liquid. This approximation is a fairly good one, especially for low superheat evaporation (see Plesset & Prosperetti 1976).

The heat transfer is described by the time-dependent energy equation which includes conduction and convection. Unlike the previous studies by other authors, we include the transient term since the Péclet number is large for this problem. This transient term is largely responsible for the local energy absorption in the drop at the early stage, resulting in a lower total heat transfer rate. The energy equation is solved for both the continuous phase and the liquid portion of the dispersed phase with the convective velocity taken from the fluid flow solution. As a result we have to solve the heat transfer problem numerically since an analytical solution does not appear to be possible.

The governing equation for the temperature field is as follows:

$$\frac{\partial T_i}{\partial t} + \boldsymbol{u}_i \cdot \boldsymbol{\nabla} T_i = \left(\frac{k}{\rho c_p}\right)_i \nabla^2 T_i \quad (i = 1, 2 \text{ no sum}), \tag{2}$$

where T_i is the temperature, t the time, $\boldsymbol{u}_i$ the velocity, k_i the conductivity, ρ_i the density and c_{p_i} the specific heat. The subscripts 1 and 2 refer to the continuous phase and the liquid portion of the dispersed phase respectively. These subscripts will not be used when not needed, particularly in general reference to both the liquid phases. The boundary and interface conditions are summarized as follows: (i) uniform temperature T_∞ at infinity; (ii) continuity of temperature at the liquid–liquid interface 1–2; (iii) continuity of heat flux at the liquid–liquid interface 1–2; (iv) zero heat flux (no heat transfer) at the interface 1–3 because of negligible conductivity of

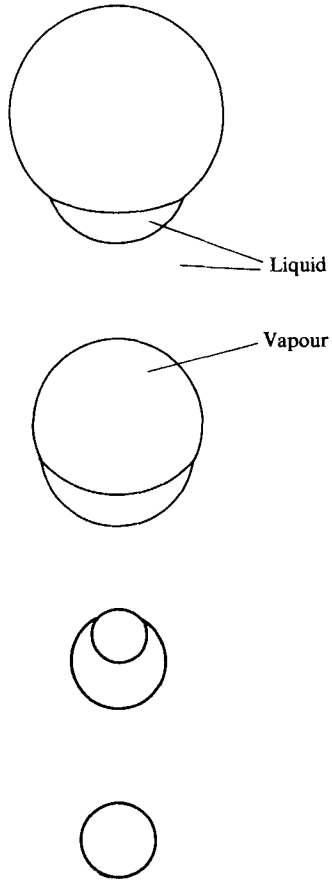

FIGURE 1. A schematic of the compound drop undergoing change of phase.

the vapour phase; and (v) constant temperature T_s (equilibrium temperature corresponding to the hydrostatic pressure) at the liquid–vapour interface 2–3.

After solving the energy equation, we can obtain the entire temperature field for both the continuous- and dispersed-phase fluids and also the heat transfer rate to the drop. This energy is partially absorbed by the drop as sensible heat and partially used to evaporate the drop from liquid phase to vapour phase, resulting in growth and change of shape of the drop. An energy balance at the interface 2–3 can be written as

$$\rho_{l_2}\frac{dV_{l_2}}{dt}h_{fg_2} = \int_{A_{23}} -k_{l_2}\boldsymbol{n}\cdot\boldsymbol{\nabla}T_2\,dA, \tag{3}$$

where ρ_{l_2} is the density, V_{l_2} the volume, h_{fg_2} the latent heat of vaporization, k_{l_2} the thermal conductivity, $\boldsymbol{n}$ the surface normal vector, and A_{23} the surface area.

3. Solution

In the cylindrical coordinate system (z, r), we introduce the following dimensionless variables:

$$z^* = \frac{z}{c}, \quad r^* = \frac{r}{c}, \quad t^* = \frac{U_\infty t}{c}, \quad \psi^* = \frac{\psi}{c^2 U_\infty}, \quad T_i^* = \frac{T_i - T_s}{T_\infty - T_s}; \tag{4}$$

along with the dimensionless groups

$$Re_i = \frac{cU_\infty}{\nu_i}, \quad Pr_i = \left(\frac{\mu c_p}{k}\right)_i, \quad Pe_i = Pr_i Re_i, \tag{5}$$

where c, the radius of the contact circle, is used as a lengthscale which changes with time. The stream function, ψ, along with U_∞ represent the flow field derived in Part 1. The energy equation (2) can now be written in the following dimensionless form:

$$\frac{\partial T}{\partial t} + u\frac{\partial T}{\partial z} + v\frac{\partial T}{\partial r} = \frac{1}{Pe}\left(\frac{\partial^2 T}{\partial z^2} + \frac{\partial^2 T}{\partial r^2} + \frac{1}{r}\frac{\partial T}{\partial r}\right), \tag{6}$$

where the asterisks have been dropped and the subscripts $i = 1, 2$ are implied for the respective liquid phases.

Boundary and interface conditions

(i) At the far field, the temperature has the free-stream value, T_∞;

$$T_1 = 1. \tag{7}$$

(ii) At the axis of symmetry;

$$\frac{\partial T_1}{\partial r} = 0, \quad \frac{\partial T_2}{\partial r} = 0. \tag{8}$$

(iii) At the liquid–liquid interface 1–2, the temperature and heat flux are continuous;

$$T_1 = T_2, \quad k_1 \boldsymbol{n}\cdot\nabla T_1 = k_2 \boldsymbol{n}\cdot\nabla T_2. \tag{9}$$

(iv) At the liquid–vapour interface 1–3, negligible heat conductivity of the vapour phase is assumed;

$$\boldsymbol{n}\cdot\nabla T_1 = \frac{\partial T_1}{\partial n} = 0. \tag{10}$$

(v) At the liquid–vapour interface 2–3, the temperature is taken to be uniform at the equilibrium value, T_s, corresponding to the hydrostatic pressure;

$$T_2 = 0. \tag{11}$$

The Péclet number in the case we are studying is significantly large, therefore the left-hand side of (6) cannot be ignored. As a result, we have to turn to a numerical method for its solution, which is given in the next section.

3.1. *Numerical analysis*

Since we have solved the Stokes equation in the toroidal coordinate system in Part 1, it would seem natural to use the same coordinate transformation for the energy equation (6). However, the energy equation written in toroidal coordinates with the convection and conduction terms can be very tedious and cumbersome. Therefore, we shall use a generalized curvilinear coordinate transformation instead, which has the advantage that it can conform with any type of irregular geometry and transform it into a suitably spaced rectangular grid so that the finite-difference method can be easily applied. We introduce a computational domain (χ, ζ, τ) in a

curvilinear coordinate system which is related to the physical domain (z, r, t) as follows:

$$z = z(\chi, \zeta, \tau), \quad r = r(\chi, \zeta, \tau), \tag{12}$$

$$\begin{bmatrix} \partial_z \\ \partial_r \\ \partial_t \end{bmatrix} = \begin{bmatrix} \chi_z & \zeta_z & 0 \\ \chi_r & \zeta_r & 0 \\ \chi_t & \zeta_t & 1 \end{bmatrix} \begin{bmatrix} \partial_\chi \\ \partial_\zeta \\ \partial_\tau \end{bmatrix}. \tag{13}$$

Also

$$\chi = \chi(z, r, t), \quad \zeta = \zeta(z, r, t), \tag{14}$$

$$\begin{bmatrix} \partial_\chi \\ \partial_\zeta \\ \partial_\tau \end{bmatrix} = \begin{bmatrix} z_\chi & r_\chi & 0 \\ z_\zeta & r_\zeta & 0 \\ z_\tau & r_\tau & 1 \end{bmatrix} \begin{bmatrix} \partial_z \\ \partial_r \\ \partial_t \end{bmatrix}. \tag{15}$$

Using the Jacobian transformation,

$$J = \frac{\partial(\chi, \zeta)}{\partial(z, r)} = \chi_z \zeta_r - \chi_r \zeta_z = (z_\chi r_\zeta - z_\zeta r_\chi)^{-1} \tag{16}$$

we obtain the following relationships between the transformation metrics:

$$\chi_z = J r_\zeta; \quad \zeta_z = -J r_\chi; \quad \chi_r = -J z_\zeta; \quad \zeta_r = J z_\chi, \tag{17}$$

$$\chi_t = -(z_\tau \chi_z + r_\tau \chi_r); \quad \zeta_t = -(z_\tau \zeta_z + r_\tau \zeta_r). \tag{18}$$

The transformation of the energy equation (6) from cylindrical coordinates (z, r, t) to generalized curvilinear coordinates (χ, ζ, τ) encompasses the use of (13) together with the following equations:

$$\frac{\partial^2 T}{\partial z^2} = \chi_z^2 \frac{\partial^2 T}{\partial \chi^2} + 2\chi_z \zeta_z \frac{\partial^2 T}{\partial \chi \, \partial \zeta} + \zeta_z^2 \frac{\partial^2 T}{\partial \zeta^2} + \chi_{zz} \frac{\partial T}{\partial \chi} + \zeta_{zz} \frac{\partial T}{\partial \zeta}, \tag{19}$$

$$\frac{\partial^2 T}{\partial r^2} = \chi_r^2 \frac{\partial^2 T}{\partial \chi^2} + 2\chi_r \zeta_r \frac{\partial^2 T}{\partial \chi \, \partial \zeta} + \zeta_r^2 \frac{\partial^2 T}{\partial \zeta^2} + \chi_{rr} \frac{\partial T}{\partial \chi} + \zeta_{rr} \frac{\partial T}{\partial \zeta}. \tag{20}$$

Upon substitution into (6), we have

$$\begin{aligned} Pe \frac{\partial T}{\partial \tau} = {} & (\chi_z^2 + \chi_r^2) \partial_\chi^2 T + (\zeta_z^2 + \zeta_r^2) \partial_\zeta^2 T + 2(\chi_z \zeta_z + \chi_r \zeta_r) \partial_\chi \partial_\zeta T \\ & + \left(\chi_{zz} + \chi_{rr} + \frac{\chi_r}{r} \right) \partial_\chi T + \left(\zeta_{zz} + \zeta_{rr} + \frac{\zeta_r}{r} \right) \partial_\zeta T \\ & - Pe[\chi_z(u - z_\tau) + \chi_r(v - r_\tau)] \partial_\chi T - Pe[\zeta_z(u - z_\tau) + \zeta_r(v - r_\tau)] \partial_\zeta T. \end{aligned} \tag{21}$$

Equation (21) represents the time-dependent energy equation written in curvilinear coordinates (χ, ζ, τ) with heat conduction and convection in the χ- and ζ-directions. Note that in the convection terms, we have a combination of two sets of velocities (u, v) and (z_τ, r_τ) which represent fluid velocities and grid velocities, respectively. The geometry of the drop is changing continuously as it grows in time and therefore the grid location at the current time step will not be the same as it was at the previous time step. Since the grid points are moving, their velocities are represented by z_τ and r_τ and contribute to the convective velocities in addition to the fluid velocities u and v. The total effective velocities are therefore given by $(u - z_\tau)$ and $(v - r_\tau)$ in the z- and r-directions, respectively. The equation (21) can be solved numerically by finite-difference methods which will be described in the following sections.

3.1.1. *Time differencing*

We apply first-order Euler implicit time differencing to (21) and obtain

$$Pe(T-T^{n-1}) = \Delta\tau(\chi_z^2+\chi_r^2)\,\partial_\chi^2 T+\Delta\tau(\zeta_z^2+\zeta_r^2)\,\partial_\zeta^2 T+2\Delta\tau(\chi_z\zeta_z+\chi_r\zeta_r)\,\partial_\chi\partial_\zeta T$$
$$+\Delta\tau\left(\chi_{zz}+\chi_{rr}+\frac{\chi_r}{r}\right)\partial_\chi T+\Delta\tau\left(\zeta_{zz}+\zeta_{rr}+\frac{\zeta_r}{r}\right)\partial_\zeta T-\Delta\tau Pe[\chi_z(u-z_\tau)$$
$$+\chi_r(v-r_\tau)]\,\partial_\chi T-\Delta\tau Pe[\zeta_z(u-z_\tau)+\zeta_r(v-r_\tau)]\,\partial_\zeta T, \tag{22}$$

where T^{n-1} denotes the temperature at the previous time step, T denotes the temperature at the current time step and $\Delta\tau$ denotes the time interval. The advantage of using implicit time differencing is to enhance the stability of the numerical solution.

3.1.2. *Spatial differencing*

The above section describes the method to advance the solution one time step. In order to solve (22), one also needs to approximate the spatial derivatives ∂_χ, ∂_ζ, ∂_χ^2, ∂_ζ^2, $\partial_\chi\partial_\zeta$ by finite differences.

(i) The diffusion terms associated with the second-order spatial derivatives ∂_χ^2, ∂_ζ^2, $\partial_\chi\partial_\zeta$ are approximated by central difference as follows:

$$\partial_\chi^2 q \approx \frac{1}{\Delta\chi^2}(q_{i+1,j}-2q_{i,j}+q_{i-1,j}), \tag{23}$$

$$\partial_\zeta^2 q \approx \frac{1}{\Delta\zeta^2}(q_{i,j+q}-2q_{i,j}+q_{i,j-1}), \tag{24}$$

$$\partial_\chi\partial_\zeta q \approx \frac{1}{4\Delta\chi\,\Delta\zeta}(q_{i+1,j+1}-q_{i+1,j-1}-q_{i-1,j+1}+q_{i-1,j-1}). \tag{25}$$

(ii) The convection terms associated with the first-order spatial derivatives ∂_χ and ∂_ζ are normally approximated by central difference:

$$\frac{\partial q}{\partial\chi} \approx \frac{1}{2\Delta\chi}(q_{i+1,j}-q_{i-1,j}), \tag{26}$$

$$\frac{\partial q}{\partial\zeta} \approx \frac{1}{2\Delta\zeta}(q_{i,j+1}-q_{i,j-1}). \tag{27}$$

From past experience, it has been found that the pure central-difference approximation to the convective terms described above will often render the numerical scheme unstable. The reason is that it does not take into account the history effect of the flow field but merely takes the difference between the two adjacent points without knowing where the flow information comes from. The central difference also produces a tridiagonal matrix which is non-diagonal dominant and is likely to cause numerical instability.

In the present study, first-order upwind-differencing is used for all convective fluxes. Numerically the upwind method will yield a tridiagonal matrix which is diagonal dominant and therefore unconditionally stable. Physically the upwind method chooses either forward or backward differencing depending on whether the flow is moving to the right or to the left. This is a very important aspect to describe

the flow characteristic to allow a proper transfer of information. The first-order upwind-differencing can be summarized as follows:

$$\frac{\partial q}{\partial \chi} = \frac{q_{i+1} - q_{i-1}}{2\Delta\chi} - \tfrac{1}{2}\Delta\chi\,\Delta_i \frac{q_{i+1} - 2q_i + q_{i-1}}{\Delta\chi^2} \tag{28}$$

where

$$\Delta_i = \operatorname{sgn} u = \begin{cases} 1. & \text{if} \quad u > 0 \\ -1 & \text{if} \quad u < 0. \end{cases} \tag{29}$$

A second-order upwind-differencing for the convective fluxes could have been used to improve the accuracy and to be compatible with the second-order central differencing for the diffusive fluxes. The reason for using the first-order upwind-differencing here is to simplify the programming effort and to reduce the computer time. Besides, we are using a very fine grid in our computation and the accuracy lost in using the first-order approximation will be minimized.

By defining

$$A = \Delta\tau(\chi_z^2 + \chi_r^2), \tag{30}$$

$$B = \Delta\tau(\zeta_z^2 + \zeta_r^2), \tag{31}$$

$$C = \Delta\tau(\chi_z \zeta_z + \chi_r \zeta_r), \tag{32}$$

$$D = \Delta\tau\left(\chi_{zz} + \chi_{rr} + \frac{\chi_r}{r}\right), \tag{33}$$

$$E = \Delta\tau\left(\zeta_{zz} + \zeta_{rr} + \frac{\zeta_r}{r}\right), \tag{34}$$

$$F = \Delta\tau Pe[\chi_z(u - z_\tau) + \chi_r(v - r_\tau)], \tag{35}$$

$$G = \Delta\tau Pe[\zeta_z(u - z_\tau) + \zeta_r(v - r_\tau)], \tag{36}$$

and applying the central-differencing approximation for the diffusion terms and the upwind-differencing approximation for the convection terms, one obtains

$$\begin{aligned} &-(2A + 2B + |F| + |G| + Pe)\,T_{i,j} + \tfrac{1}{2}(2A - D + |F| + F)\,T_{i-1,j} + \tfrac{1}{2}(2A + D + |F| - F)\,T_{i+1,j} \\ &\quad + \tfrac{1}{2}(2B - E + |G| + G)\,T_{i,j-1} + \tfrac{1}{2}(2B + E + |G| - G)\,T_{i,j+1} \\ &\quad + \frac{C}{2}(T_{i+1,j+1} - T_{i+1,j-1} + T_{i-1,j-1} - T_{i-1,j+1}) + PeT_{i,j}^{m-1} = 0. \end{aligned} \tag{37}$$

The strongly implicit equation (37) requires a nine-point scheme for each point (i,j):

$$\begin{bmatrix} (i-1,j+1) & (i,j+1) & (i+1,j+1) \\ (i-1,j) & (i,j) & (i+1,j) \\ (i-1,j-1) & (i,j-1) & (i+1,j-1) \end{bmatrix},$$

and the resulting matrix for the entire computational domain can be very large if one tries to solve it with a standard Gaussian elimination technique. This method is also very inefficient and time consuming and therefore iteration methods are normally used instead. One of these is the modified strongly implicit (MSI) method which has been claimed to be one of the most efficient iteration methods for solving field

equations. Here, we use successive line over-relaxation (SLOR) which requires only solution of a tridiagonal matrix and can be described as follows:

$$-\tfrac{1}{2}(2A-D+|F|+F)\,T^{m+1}_{i-1,j}-\tfrac{1}{2}(2A+D+|F|-F)\,T^{m+1}_{i+1,j}+(2A+2B+|F|+|G|+Pe)\,T^{m+1}_{i,j}$$
$$=\tfrac{1}{2}(2B-E+|G|+G)(T^{m+1}_{i,j-1})'+\tfrac{1}{2}(2B+E+|G|-G)\,T^{m}_{i,j+1}$$
$$+\tfrac{1}{2}C[T^{m}_{i+1,j+1}-(T^{m+1}_{i+1,j-1})'+T(^{m+1}_{i-1,j-1})'-T^{m}_{i-1,j+1}]+PeT^{n-1}_{i,j}, \tag{38}$$

$$(T^{m+1}_{i,j})'=(T^{m}_{i,j})'+\Omega[T^{m+1}_{i,j}-(T^{m}_{i,j})'], \tag{39}$$

where Ω is the relaxation parameter, $T^{m+1}_{i,j}$ the Gauss–Seidel solution, $(T^{m+1}_{i,j})'$ the relaxation solution, m the iteration index.

In the present case, we choose a grid size of 201×301 with 201 points in the χ-direction and 301 points in the ζ-direction for all drop configurations. Grids points are clustered at the interfaces in the ζ-direction to provide enough resolution to capture the thermal boundary layer. In order to save computational time, which can be enormous for this problem, we choose to fix the geometry of the drop with a one-degree increment of the interface angle at each step, then calculate the time step required for the corresponding angle increment. Because of the implicit scheme, we are able to choose a larger time step without worrying about the instability problem. Equations (38) and (39) are iterated until reasonable convergence is obtained for each drop configuration.

3.2. *Geometrical relationships*

3.2.1. *Interfacial tension and contact angles*

Since the drop is assumed to move slowly and since it is considered to be sufficiently small, the normal stress variation has a negligible effect. We therefore treat the drop as if it is a static compound drop. With this assumption, we can determine the equilibrium configuration of the drop by balancing the surface tension forces at the interfaces. This leads to the following relationships between the surface tensions and the contact angles (see Johnson & Sadhal 1985):

$$\cos\theta_1=\frac{1}{2}\left(\frac{\sigma_{12}}{\sigma_{13}}\right)\left[\left(\frac{\sigma_{23}}{\sigma_{12}}\right)^2-\left(\frac{\sigma_{13}}{\sigma_{12}}\right)^2-1\right], \tag{40}$$

$$\cos\theta_2=\frac{1}{2}\left(\frac{\sigma_{12}}{\sigma_{23}}\right)\left[\left(\frac{\sigma_{13}}{\sigma_{12}}\right)^2-\left(\frac{\sigma_{23}}{\sigma_{12}}\right)^2-1\right], \tag{41}$$

where θ_1 and θ_2 are the contact angles as shown in figure 2 along with θ_3. Thus, for constant values of the surface tensions, θ_1, θ_2 and θ_3 are also constant. This implies that the relative angles between the three interfaces are constant no matter what shape the drop takes. The angles that the interfaces make with the plane of the contact circle, η_{13}, η_{12} and η_{23} (see figure 2), do change with growth. But the angular velocities $\dot{\eta}$ at the three interfaces are the same ($\dot{\eta}_{13}=\dot{\eta}_{12}=\dot{\eta}_{23}$). For the problem of pentane rising in glycerol, we estimated $\sigma_{12}=45$ dyn/cm, $\sigma_{13}=61$ dyn/cm, $\sigma_{23}=18$ dyn/cm; therefore we calculated the values of θ_1, θ_2, θ_3 to be 171°, 32°, and 157°, respectively. These values were used to determine the shape of the drop at any instant of time.

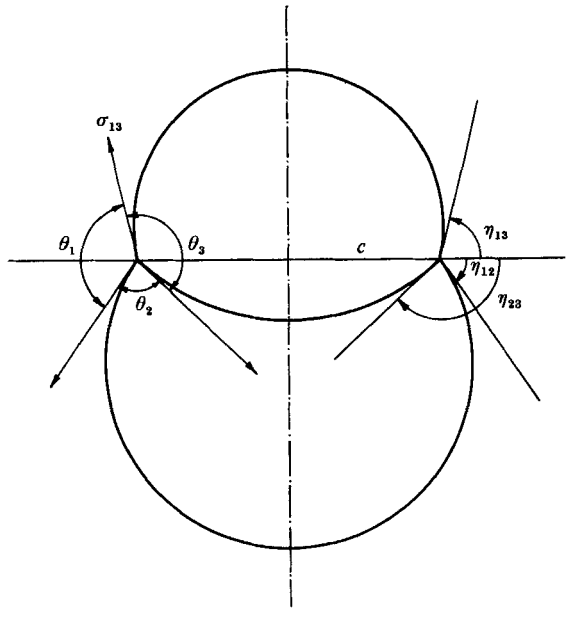

FIGURE 2. A schematic showing the geometrical relationships.

3.2.2. *Liquid and vapour volume relationships*

By defining V_l to be the volume of liquid phase and V_v to be the volume of vapour phase, one can derive from elementary geometry:

$$V_l^* = \left[\frac{2+\cos\eta_{12}(3-\cos^2\eta_{12})}{|\sin\eta_{12}|^3} - \frac{2+\cos\eta_{23}(3-\cos^2\eta_{23})}{|\sin\eta_{23}|^3}\right], \tag{42}$$

$$V_v^* = \left[\frac{2+\cos\eta_{23}(3-\cos^2\eta_{23})}{|\sin\eta_{23}|^3} + \frac{2+\cos\eta_{13}(3-\cos^2\eta_{13})}{|\sin\eta_{13}|^3}\right]. \tag{43}$$

Here the volumes have been non-dimensionalized by using the contact-circle radius as a lengthscale; that is,

$$V_l^* = \frac{3V_l}{\pi c^3}, \quad V_v^* = \frac{3V_v}{\pi c^3}. \tag{44}$$

3.3. *Growth history*

The total heat transfer rate at interface 2–3 can be written as

$$\dot{Q} = \int -k_2 \boldsymbol{n}\cdot\nabla T_2 \,\mathrm{d}A = -\int k_2 \frac{\partial T_2}{\partial n} 2\pi r \,\mathrm{d}s \tag{45}$$

or

$$\dot{Q} = -2\pi k_2 c(T_\infty - T_s)\int \frac{\partial T_2^*}{\partial n^*} r^* \,\mathrm{d}s^*, \tag{46}$$

where the asterisk denotes non-dimensional quantities. This may be non-dimensionalized in the form of a Nusselt number,

$$Nu = \frac{\dot{Q}}{2\pi k_2 c(T_\infty - T_s)} = -\int \frac{\partial T_2^*}{\partial n^*} r^* \,\mathrm{d}s^*. \tag{47}$$

The total heat transferred at interface 2–3 is used to evaporate a portion of the dispersed-phase liquid (fluid 2). Thus,

$$\dot{Q} = \rho_2 \frac{\mathrm{d}V_2}{\mathrm{d}t} h_{\mathrm{fg}_2}. \tag{48}$$

By using non-dimensional variables,

$$V_2^* = \frac{V_2}{\frac{1}{3}\pi c^3}, \quad t^* = \frac{U_\infty t}{c}, \tag{49}$$

(48) becomes

$$\frac{\mathrm{d}V_2^*}{\mathrm{d}t^*} = 6 \frac{c_{p_2}(T_\infty - T_s)}{h_{\mathrm{fg}_2}} \frac{Nu}{Pr_2 Re_2}. \tag{50}$$

The mass lost from the liquid phase goes into the vapour phase by the relationship

$$\mathrm{d}V_v^* = -\left(\frac{\rho_l}{\rho_v}\right)_2 \mathrm{d}V_l^*. \tag{51}$$

The total heat absorbed by the drop is given by

$$Q = \int \dot{Q}\, \mathrm{d}t \tag{52}$$

which may be non-dimensionalized to give

$$Q^* = \frac{Q}{2\pi\rho_2 c_{p_2} c^3 (T_\infty - T_s)} = \int \frac{Nu}{Pr_2 Re_2} \mathrm{d}t^*. \tag{53}$$

3.4. *Effect of hydrostatic pressure*

When the drop is first introduced into a column of the continuous phase, it is subjected to a pressure which is equal to the hydrostatic pressure of the fluid column. Assuming the pressure jump across the interface of the drop to be negligible, the vapour pressure is the same as the outside hydrostatic pressure. The equilibrium temperature corresponding to the vapour pressure can be determined by the Clausius–Clapeyron equation. As the drop rises through the column, the hydrostatic pressure drops and so does the equilibrium temperature, while the batch temperature is constant. Therefore the superheat $(T_\infty - T_s)$ will not be constant but will increase gradually to higher values. The superheat temperature given here is the value when the drop first enters the column at the bottom. The superheat temperature increases gradually from the bottom to the top of the column. This effect is also taken into account in the present analysis.

3.5. *Calculation procedures*

The following iterative procedure is adopted:

(i) Assuming an initial configuration to consist of a mostly liquid drop by giving an initial volume ratio (V_l/V_v), solve for η_{23}, η_{12} and η_{13}.

(ii) With known geometry, a grid is generated.

(iii) The growth velocities, $\dot{c}$ and $\dot{\eta}$, and the translational velocity, U_∞ are calculated.

(iv) The velocity field of the system due to translation and growth is calculated from the analytical solution of Part 1.

(v) The temperature field is solved for.

(vi) The non-dimensional heat transfer rate,

$$Nu = \frac{\dot{Q}}{2\pi k_2 c(T_\infty - T_s)}, \tag{54}$$

is calculated.

(vii) The volume of the evaporated liquid,

$$\mathrm{d}V_l^* = 6\frac{c_{p_2}(T_\infty - T_s)}{h_{fg_2}}\frac{Nu}{Pr_2 Re_2}\mathrm{d}t^*, \tag{55}$$

is found.

(viii) The volume increment of the vapour phase,

$$\mathrm{d}V_v^* = -\left(\frac{\rho_l}{\rho_v}\right)_2 \mathrm{d}V_l^*, \tag{56}$$

is obtained.

(ix) Total heat absorbed by the drop,

$$Q^* = \frac{Q}{2\pi\rho_2 c_{p_2} c^3(T_\infty - T_s)}\int \frac{Nu}{Pr_2 Re_2}\mathrm{d}t^*, \tag{57}$$

is calculated.

(x) The new volume ratio (V_l/V_v) is obtained from the relationship:

$$\left[\frac{V_l^*}{V_v^*}\right]_{new} = \frac{V_{l_{old}}^* + \mathrm{d}V_l^*}{V_{v_{old}}^* + \mathrm{d}V_v^*}. \tag{58}$$

(xi) We go to step (i) and iterate until the drop has almost evaporated.

This procedure gives the complete evaporation history of the drop.

4. Results and discussion

The procedure outlined in the last sections is used to calculate the time history of a pentane drop immersed in a bath of glycerol. The large computational expense has prevented us from doing a parametric study to investigate the sensitivity of the temperature variation with various sets of conditions using different fluids. This is mainly because the configuration of the drop is highly dependent on the fluid systems. We have chosen the case of a pentane drop immersed in glycerol for our study since this case was described experimentally by Tochitani *et al.* (1977*a*, *b*) and some of the crucial data for the fluid properties can be obtained. In fact, our examples closely follow the experiments described in those references so that we can compare the results of present analysis with the experimental data. We choose two representative cases of drops with initial diameters of 0.8 mm and 1.4 mm immersed in a column of glycerol of height 0.5 m. The column was maintained at superheat temperatures $(T_\infty - T_s)$ of 3.1, 6.1 and 12.1 K. Here T_∞ is the bath temperature and T_s is the equilibrium temperature corresponding to the hydrostatic pressure of the fluid column when the drop first enters the column at the bottom. The fluid flow and heat transfer history are calculated for all three cases and presented in the following sections.

4.1. *Comparison of results with experimental data*

The computational results are compared with the experimental data obtained by Tochitani *et al.* (1977*a*, *b*) in order to examine the accuracy of the present analysis.

The shape calculations for the drop are checked by comparing the area ratio and the half-opening angle. The fluid mechanics and heat transfer results can be verified by comparing the velocity of rise and the heat transfer coefficient.

4.1.1. *Area ratio and half-opening angle*

The area ratio is A_L/A_T, where A_L is the surface area of liquid–liquid interface 1–2 and A_T is the total surface area of the two-phase drop. The half-opening angle β is equal to $(\pi-\eta_{13})$ here. Tochitani *et al.* (1977*a*, *b*) measured the area ratio and half-opening angle so that they could calculate heat transfer coefficients using their formulation. Figures 3 and 4 show the area ratio and half-opening angle β versus the vaporization ratio X for the two drop sizes with $(T_\infty - T_s) = 3.1$ K. The vaporization ratio X is M_{dv}/M_d, where M_{dv} is the mass of the drop in vapour phase and M_d is the total mass of the drop. The dashed lines represent the results of the present analysis and the solid lines represent the results by Tochitani *et al.* (1977*a*, *b*). The present analysis gives a better agreement with experimental data than the results by Tochitani *et al.* (1977*a*, *b*). The reason is that they had assumed the drop to be of spherical shape with the vapour phase occupying the upper portion and the liquid phase staying at the bottom portion in order to simplify the analysis. The accuracy of this approximation depends on the fluid system being used. In their experiment, they also noted that the profile of the unevaporated liquid of the drop jutted out from the spherical boundary of the vapour with the continuous phase. In other words, the drop is far from being of spherical shape. This resulted in the discrepancy between their analytical results and experimental data. We also note that the area ratio and the half-opening angle are independent of the drop size and the amount of superheat $(T_\infty - T_s)$; these are functions of the drop geometry which is determined by the three surface tensions σ_{12}, σ_{13} and σ_{23} as described in the previous section.

4.1.2. *Velocity of rise*

The calculation for the drag force was used to determine the instantaneous velocity of rise by balancing the drag force and the buoyancy force, assuming a quasi-steady state. Figure 5 shows the velocity versus vaporization ratio X. The present results are compared with experimental data given by Tochitani *et al.* (1977*a*, *b*) for two initial drop diameters of 0.8 mm and 1.4 mm. Tochitani *et al.* (1977*b*) measured the velocities of rise experimentally and compared them with terminal velocities from Stokes drag for a solid sphere (represented by solid lines) and the Rybczinski–Hadamard drag for a gas bubble (represented by dashed lines). The present analysis agrees with the results in the previous section of the drag calculations which fall between the two limiting cases of a solid sphere and a gas bubble. In the early state when the drop is mostly liquid, the predicted velocity of rise tends to agree with the theory for a solid sphere. In the final state when the drop is mostly vapour, the predicted velocity tends to agree with the theory for a gas bubble. The experimental data follows more closely with the theory for a solid sphere. As pointed out by Tochitani *et al.* (1977*a*, *b*), this is probably due to the contamination of the bubble surface so that to some extent it acts more like a solid sphere. Also, the column wall might have some influence on the velocity. The wall effect was noted by Tochitani *et al.* (1977*a*, *b*) to be $[1-(D/L)^{1.5}]$, which has a value of 0.94 in this case. By multiplying the present result with that factor, we obtained a better agreement with the experimental data.

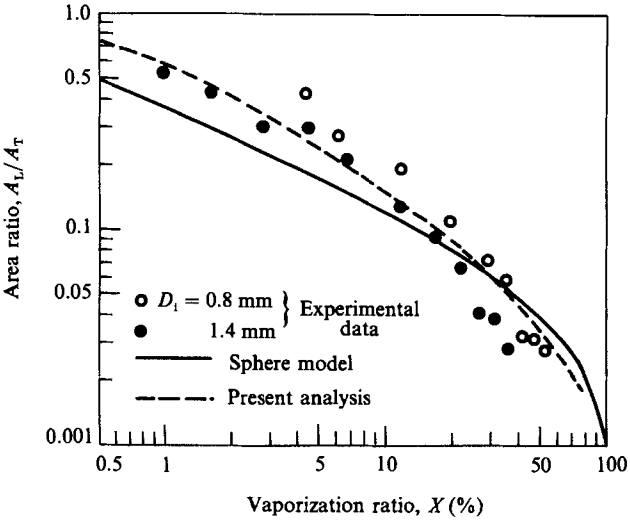

FIGURE 3. Area ratio *vs.* vaporization ratio ($\Delta T = 3.1$ K).

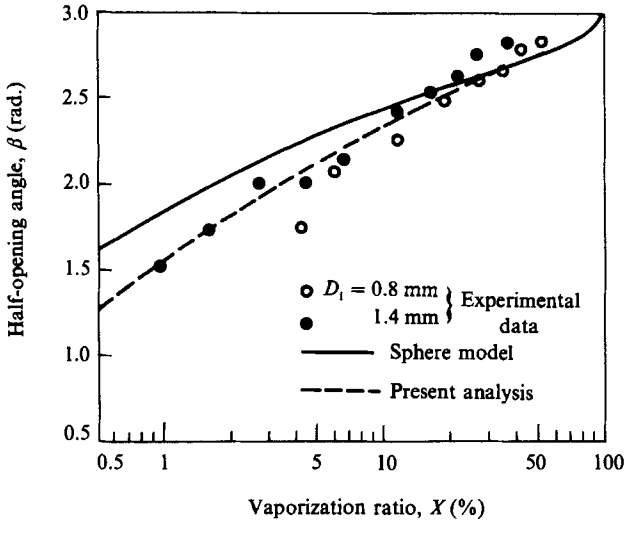

FIGURE 4. Half-opening angle *vs.* vaporization ratio ($\Delta T = 3.1$ K).

4.1.3. *Average heat transfer coefficient*

The average heat transfer coefficient is defined here as $\dot{Q}/[A_T(T_\infty - T_s)]$, where $\dot{Q}$ is the instantaneous rate of heat transfer from the continuous phase to the dispersed phase, A_T is the total surface area of the drop in contact with the dispersed phase. In the experiment by Tochitani *et al.* (1977*b*) the cumulative heat Q transferred into the two-phase drop was obtained by using a dilatometer to measure the volume of the vapour phase. A polynomial which represents the dependence of Q as function of time was curve-fitted by the method of least squares. The instantaneous heat transfer rate $\dot{Q}$ can then be obtained by differentiation of the polynomial. In the present analysis, the heat transfer rate $\dot{Q}$ is obtained from the average heat flux at the liquid–vapour interface 2–3 of the dispersed phase since this is where phase

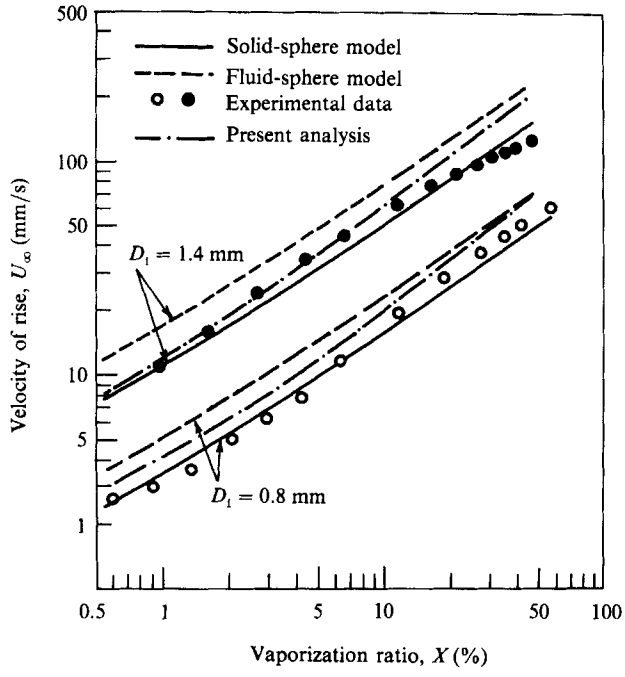

FIGURE 5. Velocity of rise *vs.* vaporization ratio ($\Delta T = 3.1$ K).

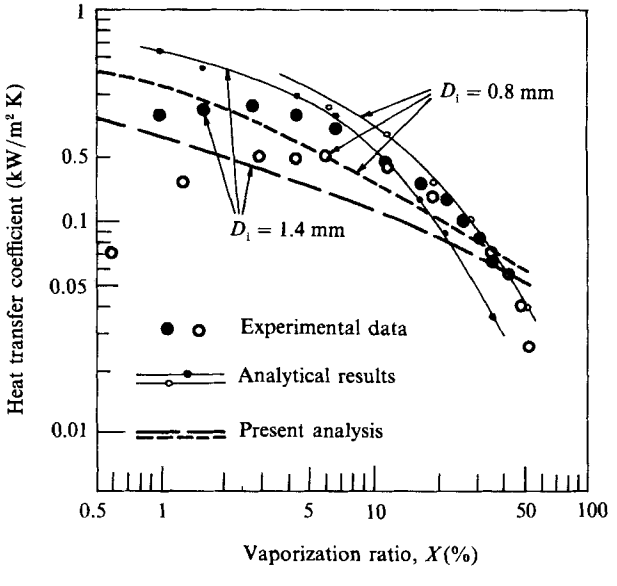

FIGURE 6. Heat transfer coefficient *vs.* vaporization ratio ($\Delta T = 3.1$ K).

change occurs. In Tochitani *et al.*'s analysis, the heat transfer rate $\dot{Q}$ is calculated at the liquid–liquid interface 1–2 since the dispersed phase was not taken into account. Figure 6 shows the heat transfer coefficient for two drop sizes of 0.8 mm and 1.4 mm initial diameter with a superheat temperature of 3.1 K. The two solid lines represent the analytical heat transfer coefficients at the liquid–liquid interface given by

Tochitani *et al.* (1977*b*). Their results are higher than the experimental data since they neglected the resistance of the liquid phase of the drop. The result of the present analysis is lower than that of Tochitani's since we take into account the liquid layer of the dispersed phase, resulting in better agreement with the experimental data. For an unexplainable reason, the measured heat transfer coefficient for the 1.4 mm diameter drop is higher than for the 0.8 mm diameter drop, which is in contradiction with the theory that the heat transfer coefficient is inversely proportional to the size of the drop as shown in the present analysis. This was also verified by Sideman, Hirsch & Gat (1965).

4.2. *Time history of the drop*

The time history of the average Nusselt number, defined as $Nu = \dot{Q}/[2\pi k_2 r_0(T_\infty - T_s)]$, is shown in figure 7 for three superheat temperatures of 3.1, 6.1 and 12.1 K, respectively. Here we use the non-dimensional time $t' = U_0 t/r_0$, where U_0 is the initial velocity of the compound drop and r_0 is the initial radius of the vapour bubble.

On each figure, the average Nusselt numbers are presented for the liquid–liquid interface (Nu_o) and the liquid–vapour interface (Nu_i). When the drop is first immersed into a higher temperature fluid, there is a very large temperature gradient at the liquid–liquid interface because of two different fluid temperatures, resulting in very high value of Nu_o. A short time later, a very thin conduction layer in the region of the liquid–liquid interface 1–2 begins to form due to the transient effect and the energy of the external fluid is transferred to the drop. This is responsible for the steep drop of the heat transfer coefficient Nu_o. Meanwhile at the liquid–vapour interface 2–3 of the drop, the temperature of the fluid begins to increase owing to the energy absorbed from the external fluid, and we see a rapid rise of Nu_i. The two Nusselt number Nu_o and Nu_i approach each other at a larger time since the transient effect is no longer important. The area under Nu_o can be interpreted as the cumulative amount of energy transferred to the drop from the continuous phase. The area under Nu_i can be interpreted as the energy transferred from the drop into the vapour phase. The area between the two curves is the energy accumulated by the liquid phase of the drop. Initially the area difference between the two curves is large, which shows that a large amount of energy is being absorbed to warm up the drop, leaving little energy for evaporation. As time passes, this area decreases gradually, which means that the transient effect is diminishing and the energy absorbed by the drop from the continuous phase is transferred directly to the vapour phase by evaporation.

The behaviour of Nu_i is similar for all three superheat temperatures but it is not so for Nu_o. For 3.1 K superheat, Nu_o drops quickly at the beginning and then levels off for a while, followed by a gradual decrease. For 6.1 K superheat, Nu_o drops quickly at the beginning, then it rises, followed by a gradual drop. For 12.1 K superheat, the rise is even higher. This can be explained by internal circulation of the drop. As the drop first makes contact with the continuous phase, the adjacent fluid is warmed up by conduction. This results in steep drop of Nu_o while the thermal boundary layer is growing thicker. Because of the internal circulation of the dispersed phase, the warm fluid at the interface is replaced by cooler interior fluid being transported out, resulting in a rise of the Nu_o. The higher the superheat, the higher rise of Nu_o as seen in the figures. After a certain time, the fluid at the liquid–liquid interface 1–2 is being heated up again by conduction, causing Nu_o to drop again. The number of oscillation in the value of Nu_o is determined by the Péclet number, which represents the ratio of the rate of convection to the rate of conduction. This phenomenon was noted earlier by Chung, Oliver & Carleson (1985)

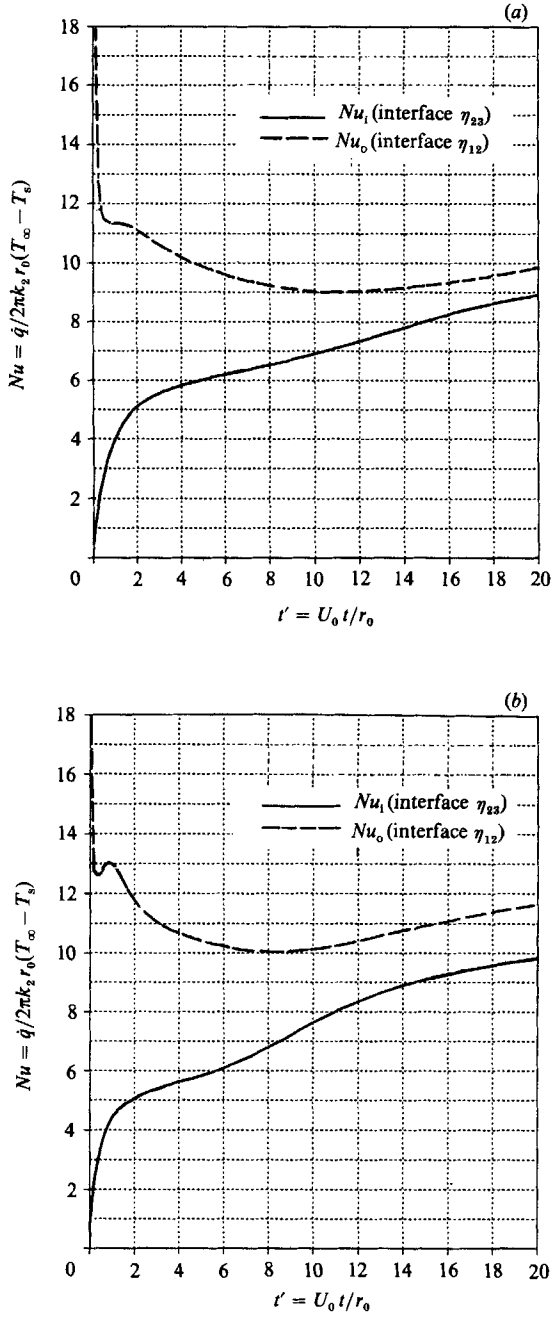

FIGURE 7 (a,b). For caption see facing page.

for single-phase drops. For problems with larger Péclet number, the convective heat is a lot stronger than the conductive heat and the cooler interior fluid will be repeatedly brought out to cool the exterior fluid, causing several such oscillations to occur before the value of Nu_0 begins to drop. In the present problem, the Péclet number is only large enough to cause one oscillation for higher superheat temperatures. We can also see the effect of the amount of superheat; the higher the

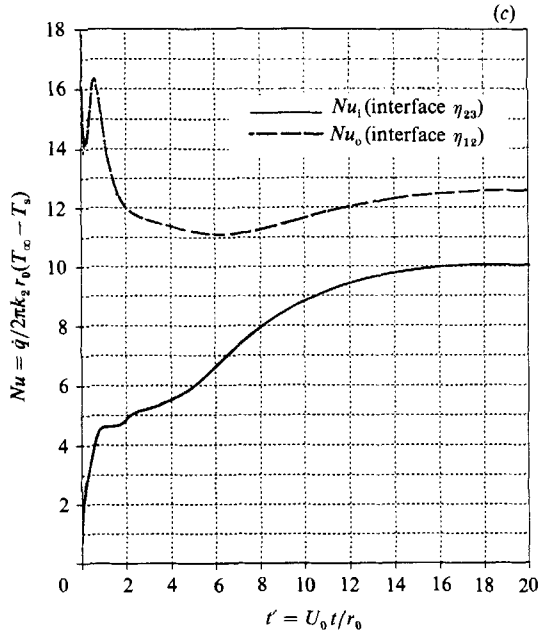

FIGURE 7. Time history of the Nusselt number: (*a*) $\Delta T = 3.1$ K; (*b*) $\Delta T = 6.1$ K; (*c*) $\Delta T = 12.1$ K ($D_i = 1.4$ mm).

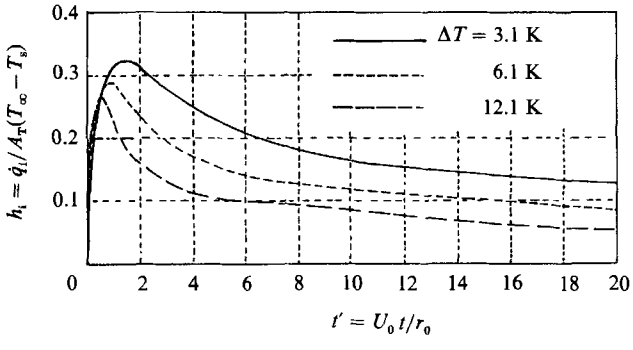

FIGURE 8. Time history of h_i (liquid–vapour interface 2–3) ($D_i = 1.4$ mm).

superheat temperature, the higher the Nusselt number. Also the value of Nu_0 oscillates at a higher peak for higher superheat. The average heat transfer coefficient h shown earlier in figure 6 for comparison with test data is $h = \dot{Q}/[A_T(T_\infty - T_s')]$, which can be calculated from the Nusselt number. Figures 8 and 9 show the time history of h_i and h_0 for the liquid–liquid interface 1–2 and liquid–vapour interface 2–3, respectively. On each figure, results are given for three superheat temperatures. We note that the total surface area A_T of the two-phase drop appearing in the denominator is not a constant but increases rapidly with time, causing a rapid drop in the values of h. For a lower superheat temperature, we get a higher value of h. This is because at any given time, a lower superheat temperature results in a lower growth rate of the drop and therefore lower total surface area A_T. The oscillation appearing in Nu_0 does not show here in the value of h_0; this is due to rapid increment of the value of A_T, which overrides the oscillation effect.

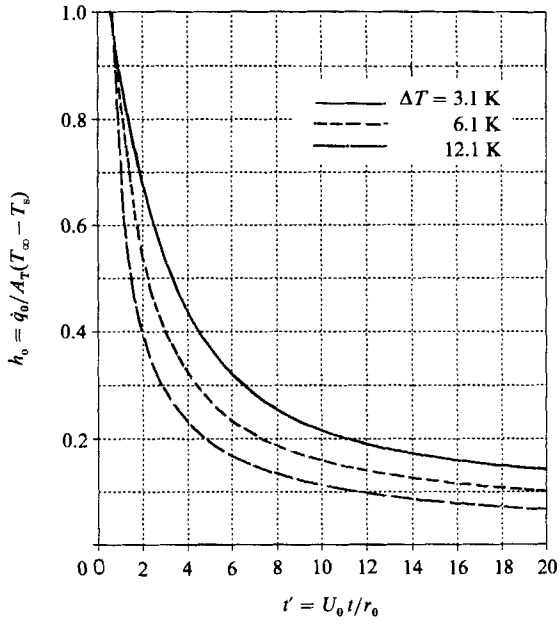

FIGURE 9. Time history of h_0 (liquid–liquid interface 1–2) (D_i = 1.4 mm).

5. Concluding remarks

In the preceding pages, we have described numerical methods to solve for the time history of a partially engulfed compound gas–liquid drop. Because of the complexity of the problem, several assumptions were made to simplify the geometry and the flow characteristics, such as small capillary number so that the interfaces of the drop remain spherical, and low-Reynolds-number flow so that the available analytical solution could be used. These assumptions limit the application of the present study to only small drops, of a radius about 1 mm. We found that the heat transfer rate increases rapidly in the early state and then stays relatively constant for the remaining time which is synchronous with the growth rate of the drop. Even though there are limits to the present study, a great deal has been learnt about the basic fluid dynamics and heat transfer of the 3-S compound drops for the entire growth process. Also the present study has significantly refined the model at the early state of the drop growth. Previous models relied heavily on the assumption of small drop liquid volume to approximate the flow field of a moving sphere and neglected the heat transfer to this liquid volume, which is only valid at the final state. For a more general case such as with moderate-Reynolds-number flow and slightly deformed drops, a fully numerical solution will be needed and it remains to be done. The present analytical model was compared with existing experimental data and the agreement between the two is reasonably good.

The authors are very grateful to the National Science Foundation for the support of this work under Grant No. CBT 83-51432. Thanks are also due to DAMTP (Cambridge University) for the availability of their research facilities to the second author (S.S.S.) who was on sabbatical leave there (5 July 1988–18 July 1989).

REFERENCES

ADAMS, A. E. S. & PINDER, K. L. 1972 Average heat transfer coefficient during the direct evaporation of a liquid drop. *Can. J. Chem. Engng* **50**, 707–713.

BATTYA, P., RAGHAVAN, R. & SEETHARAMU, K. M. 1984 Parametric studies on direct contact evaporation of a drop in an immiscible liquid. *Intl J. Heat Mass Transfer* **27**, 263–272.

CHUNG, J. N. & AYYASWAMY, P. S. 1981 Laminar condensation heat and mass transfer to a moving drop. *AiChE J.* **27**, 372–377.

CHUNG, J. N., AYYASWAMY, P. S. & SADHAL, S. S. 1984*a* Laminar condensation on a moving drop. Part 1. Singular perturbation technique. *J. Fluid Mech.* **139**, 105–130.

CHUNG, J. N., AYYASWAMY, P. S. & SADHAL, S. S. 1984*b* Laminar condensation on a moving drop. Part 2. Numerical solutions. *J. Fluid Mech.* **139**, 105–130.

CHUNG, J. N., OLIVER, D. L. R. & CARLESON, T. E. 1985 Transient heat transfer in a fluid sphere translating in an electric field. *22nd Natl Heat Transfer Conference, Denver, Colorado, August 4–7, 1985, paper* 85-HT-75.

GRADON, L. & SELECKI, A. 1977 Evaporation of a liquid drop immersed in another immiscible liquid. The case of $\sigma_c < \sigma_d$. *Intl J. Heat Mass Transfer* **20**, 459–466.

HAYAKAWA, T. & SHIGETA, M. 1974 Terminal velocity of a two phase droplet. *J. Chem. Eng. Japan* **7**, 140–142.

JACOBS, H. R. & MAJOR, B. H. 1982 The effect of noncondensible gases on bubble condensation in an immiscible liquid. *Trans. ASME* C: *J. Heat Transfer* **104**, 487–492.

JOHNSON, R. E. & SADHAL, S. S. 1985 Fluid dynamics of compound multiphase drops and bubbles. *Ann. Rev. Fluid Mech.* **17**, 289–320.

KLIPSTEIN, D. H. 1963 Heat transfer to a vaporizing immisicible drop. D.Sc. thesis, M.I.T., Cambridge, MA.

LERNER, Y. & LETAN, R. 1985 Dynamics of condensing bubbles: effects of injection frequency. *22nd Natl Heat Transfer Conference, Denver, Colorado, August 4–7, 1985, paper* 85-HT-47.

MOKHTARZADEH, M. R. & EL-SHIRBINI, A. A. 1979 A theoretical analysis of evaporating droplets in an immiscible liquid. *Intl J. Heat Mass Transfer* **22**, 27–38.

MORI, Y. H., NAGAI, K., FUNABA, H. & KOMOTORI, K. 1981 Cooling of freely falling liquid drops with a shell of an immiscible volatile liquid. *Trans. ASME* C: *J. Heat Transfer* **103**, 508–513.

OĞUZ, H. N. & SADHAL, S. S. 1987 Growth and collapse of translating compound multiphase drops: analysis of fluid mechanics and heat transfer. *J. Fluid Mech.* **179**, 105–136.

PLESSET, M. S. & PROSPERETTI, A. 1976 Flow of vapour in a liquid enclosure. *J. Fluid Mech.* **78**, 433–444.

PRAKASH, C. B. & PINDER, K. L. 1967*a* Direct contact heat transfer between two immiscible liquids during vaporization. Part I. Measurement of heat transfer coefficient. *Can. J. Chem. Engng* **45**, 210–214.

PRAKASH, C. B. & PINDER, K. L. 1967*b* Direct contact heat transfer between two immiscible liquids during vaporization. Part II. Total evaporation time. *Can. J. Chem. Engng* **45**, 215–220.

RAINA, G. K. & GROVER, P. D. 1982 Direct contact heat transfer with change of phase: theoretical model. *AIChE J.* **28**, 515–517.

RAINA, G. K. & GROVER, P. D. 1985 Direct contact heat transfer with change of phase: theoretical model incorporating sloshing effects. *AIChE. J.* **31**, 507–509.

RAINA, G. K. & WANCHOO, R. K. 1986 Direct contact heat transfer with change of phase: bubble growth and collapse. *Can. J. Chem. Engng* **64**, 393–398.

RAINA, G. K., WANCHOO, R. K. & GROVER, P. D. 1984 Direct contact heat transfer with change of phase: motion of evaporating droplets. *AIChE J.* **30**, 835–837.

SELECKI, A. & GRADON, L. 1976 Equation of motion of an expanding vapor drop in an immiscible liquid medium. *Intl J. Heat Mass Transfer* **19**, 925–929.

SIDEMAN, S., HIRSCH, G. & GAT, Y. 1965 Direct contact heat transfer with change of phase: effect of the initial drop size in three-phase heat-exchanger. *AIChE J.* **11**, 1081–1087.

SIDEMAN, S. & TAITEL, Y. 1964 Direct contact heat transfer with change of phase: evaporation of drops in an immiscible liquid medium. *Intl J. Heat Mass Transfer* **7**, 1273–1289.

SIMPSON, H. C., BEGGS, G. C. & NAZIR, M. 1974 Evaporation of a droplet of one liquid rising through a second immiscible liquid: a new theory of the heat transfer process. In *Proc. 5th Intl Heat Transfer Conf., Tokyo, 3–7 September,* vol. 5, pp. 59–63.

SUNDARARAJANA, T. & AYYASWAMY, P. S. 1984 Hydrodynamics and heat transfer associated with condensation on a moving drop: solutions for intermediate Reynolds numbers. *J. Fluid Mech.* **149**, 33–58.

TADRIST, L., SHEHU DISO, I., SANTINI, R. & PANTALONI, J. 1987 Vaporization of a liquid by direct contact in another immiscible liquid. Part I: Vaporization of a single droplet. Part II. Vaporization of rising multidroplets. *Intl J. Heat Mass Transfer* **30**, 1773–1785.

TOCHITANI, Y., MORI, Y. H. & KOMOTORI, K. 1977*a* Vaporization of single drops in an immiscible liquid. Part I. Forms and motions of vaporizing drops. *Wärme Stoffübertrag.* **10**, 51–59.

TOCHITANI, Y., NAKAGAWA, T., MORI, Y. H. & KOMOTORI, K. 1977*b* Vaporization of single liquid drops in an immiscible liquid. Part II. Heat transfer characteristics. *Wärme Stoffübertrag.* **10**, 71–79.

VUONG, S. T. & SADHAL, S. S. 1989 Growth and translation of a liquid–vapour compound drop in a second liquid. Part 1. Fluid mechanics. *J. Fluid Mech.* **209**, 617–637.